Promoting effect of CeO_2, ZrO_2 and Ce/Zr mixed oxides on Co/γ-Al_2O_3 catalyst for Fischer-Tropsch synthesis

V. Garcilaso[1*], J. Barrientos[2], L.F. Bobadilla[1], O.H. Laguna[1], M. Boutonnet[2], M.A. Centeno[1], J.A. Odriozola[1]

1 - Instituto de Ciencia de Materiales de Sevilla – Centro Mixto CSIC/Universidad de Sevilla, Avda. Américo Vespucio, 49. CP: 41092 – Seville - Spain

2 – KTH (Royal Institute of Technology), Chemical Science and Engineering, Chemical Technology, Teknikringen 42, Plant 6, SE-100 44 Stockholm (Sweden)

***Corresponding Author:** victoriagarcilaso@icmse.csic.es

Abstract

A series of cobalt-based catalysts have been synthesized using as support γ-Al_2O_3 promoted by ceria/zirconia mixed oxides with a variable Ce/Zr molar ratio. The obtained catalysts demonstrated oxide promotion results in the protection of the major textural properties, especially for Zr-rich solids. Reducibility of cobalt species was enhanced by the presence of mixed oxides. The chemical composition of the oxide promoter influenced not only physicochemical properties of final catalysts but also determined their performance during the reaction. In this sense, Zr-rich systems presented a superior catalytic performance both in total conversion and in selectivity towards long chain hydrocarbons. The observed Zr-promotion effect could be explained by two significant contributions: firstly, the partial inhibition of Co-Al spinel compound formation by the presence of Zr-rich phases which enhances the availability of Co actives site and secondly, Zr-associate acidic sites promote higher hydrocarbons selectivity.

Keywords:

Cobalt-based catalysts; oxide promoter; Zr-Ce oxides; support acidity; higher hydrocarbon selectivity; GTL.

1. Introduction

Fischer-Tropsch synthesis (FTS) is a catalytic process for transforming syngas (H_2+CO) into higher hydrocarbons, especially for liquid transportation [1–4]. Furthermore, the FTS-based technology applied by large-scale plants is either based on CH_4 reforming or coal gasification processes for syngas production. However, considering the current scenario generated by climate change, searching renewable carbon sources is a mandatory requirement to minimize the environmental impact. In this sense, coupling biomass gasification with FTS for "green" liquid fuels production is increasingly attractive [1]. Nevertheless, the CO_2 footprint would be lowered comparing conventional resources for liquid fuels production. Thus, additional efforts are required for enhancing the efficiency of the Gas to Liquid (GTL) technology at the FTS step in order to ensure its sustainability. For instance, new catalysts development is focused on overcoming H_2-deficiency when syngas is produced from residual biomass feedstock. Among the total conversion, selectivity towards biodiesel fraction of alkanes should be improved as much as possible during the FTS.

Different catalytic systems have been reported for FTS; mostly all group VIII metals are active for CO hydrogenation to hydrocarbons. According to Vannice [5], Ru, Fe, Ni, Co, and Rh have demonstrated to be more selective towards the production of high hydrocarbons. Nevertheless, the price of noble metals (NMs) makes them unprofitable at industrial level [6]. Despite this, NMs-systems are highly studied as reducibility promoters. By contrast, transition metal catalysts based on Co and Fe are more competitive than NMs-systems from the economical point of view. Consequently, these are the most used FTS catalysts besides, these have demonstrated considerable selectivity towards diesel-like hydrocarbons production, especially Co-based catalysts when the syngas stoichiometry $H_2/CO = 2.1$ is used [7]. Furthermore, it has been observed that Co-based catalysts present a superior productivity at high conversion levels after comparing Co and Fe systems [4-5,8-10].

Concerning usual Co catalysts design, a cobalt precursor is dispersed over a support surface in order to obtain metallic Co after calcination and reduction processes. Since metallic Co species are the active sites of FTS reaction. In order to increase metallic Co species dispersion to maximize the contact with gaseous reactants, high surface mesoporous materials such as

Al_2O_3, SiO_2, TiO_2 or zeolites [3] are often employed as supports. Among them γ-Al_2O_3 offers a high thermal stability and high specific surface as well as controllable textural properties.

Nevertheless, Co/Al_2O_3 systems present a strong interaction between Co-species and alumina surface through the formation of cobalt aluminate compounds [11] which is diminishing cobalt overall reducibility. To ensure metallic cobalt species availability NMs (e.g. Pt, Re and Ru) are introduced into the Co/Al_2O_3 catalysts formulation acting as a promoter [12]. This promoting effect is commonly associated to H_2-spillover from NM surface to the cobalt oxide [13]. Alumina promotion due to oxide species has been also proposed. The effect is based on allaying cobalt support compounds formation (Co-SCF), among others textural modifications [3].This is allowing a reducibility enhancement and availability of cobalt species. Apart from reducibility, oxide promoters may be controlling other catalyst features such as porosity or acidity, although there is not a general agreement about its influence. For instance, Prieto et al [14] have proposed support Lewis acid-base properties as the major contributor to activity and selectivity, showing both parameters volcano dependences. Moreover, Maitlis et al. [3] have discussed the importance of polarized surfaces for further activation of CO molecules by carbon interaction with the metallic surface together with the oxygen interaction with support Lewis acid sites.

Several studies about promoters such as Zr, Ce, La, Mg, Mn and, Ti oxides for Co/Al_2O_3 catalyst were previously reported [15]. Particularly interesting is the promoting effect of Zr in Co/Al_2O_3 catalyst, which has been studied by several authors [14-20]. Although there is not a general agreement about how Zr influence cobalt species reducibility [18]. Souza et al. [20] have explained the promotion effect of ZrO_2 combining three different properties: 1) high thermal stability, 2) protection of acid/basic Lewis sites 3) the oxophylic character of this “FTS-inactive” transition metal. In this context, Jongsomjit et al. [13] have also demonstrated the Zr-promoting effect as a consequence of cobalt reducibility enhancement, since ZrO_2 avoids Co-SCF during the reduction step prior to reaction.

Moreover, Co/Al_2O_3 catalyst promotion by cerium oxide has been also reported due to its redox properties [21]. For example, Haibo et al. [22] have demonstrated a promotion effect

of CeO_2 in Co/SiO_2 catalyst since CeO_2 increased the total amount of active carbon species on surface. Thus concentration of the chain growth unit $–CH_2$- increases which leads to an increment of FTS reactivity and a larger chain growth. Furthermore, improvement of the hydrogenation reactivity was also observed resulting in the decreasing of the coke formation. In lights of these aspects about CeO_2 promotion, solid solution formation with heteroatoms such as Zr, Fe, Zn, Cu, which has demonstrated a synergistic effect in others reactions [23-25] can be also interesting to be studied.

Selectivity towards long-chain hydrocarbons is a relevant aspect of FTS performance. Besides support physicochemical features such as acidic properties, selectivity dependence on inlet syngas composition is also demonstrated. For instance, Iglesia [8] has claimed water may increase FTS reaction rates and selectivity towards C_{5+} and olefins at low reactant pressures or conversions. This effect induced by water may be influenced by catalysts nature.

Water effects on catalytic performance of FTS have been studied not only by its influence on the reaction pathways but also considering water as a possible component of the FTS feed-stream produced from a reformer. In this sense, studies of FTS novel catalysts should be complemented by this analysis in order to establish a more accurate diagnostic of the catalytic performance, looking for selective to long chain hydrocarbons systems.

According to the previously exposed scenario, this work aims to clarify the promoting effect of Zr versus Ce oxides in Co/Al_2O_3 systems, by using several combinations of its mixed oxides. Comparison between all prepared catalysts should draw conclusions about the promoting effect based on the chemical nature of the oxide promoter.

2. Experimental

2.1 Synthesis of the catalysts

In all cases γ-Al_2O_3 spheres *Sasol® (*1.8/210) were employed as starting material. First of all alumina spheres were milled in a zirconia jar on a Retsch® PM100 equipment (20 min/500 rpm). The obtained powder was subsequently modified by precipitation method using adequate amounts of metallic precursors ($ZrO(NO_3)_2 \cdot xH_2O$ and/or $Ce(NO_3)_3 \cdot 6H_2O$, *Sigma Aldrich*) in order to obtain a 20 wt.% promoter oxide loading. Metallic salts were dissolved at RT in absolute ethanol *Merck*® (40 g/L of salt concentration) and the alumina was added under continuous stirring during 30 min. Afterwards, aqueous ammonia (1:1(v/v) H_2O /NH_3

(*30* v *% Panreac®,*) was added up to a pH 12, under continuous stirring. Then solid was separated from the liquid by filtration then dried during 24 h at 100 ºC and finally calcined at 500 ºC for 4 h. Oxide promoters have been synthesized modifying the molar percentage of Zr and Ce: 0, 10, 50, 90 and 100% of Ce, giving rise to five different support were alumina is modified.

As for catalysts preparation, a 12 wt. % of Co was loaded by means of incipient wetness impregnation using $Co(NO_3)_2.6H_2O$ from *Sigma Aldrich®*. Final powders were dried at 120 ºC for 3 h (5 ºC/min) and finally calcined at 300 ºC for 16 h in air.

Support materials were named as follows: ZrAl and CeAl for the solids promoted with the corresponding monometallic oxides (Zr and Ce, respectively) and 10CeZrAl, 50CeZrAl and 90CeZrAl for mixed systems, the number is indicating the cerium molar percentage. Accordingly, corresponding catalysts were named as CoZrAl, Co10CeZrAl, Co50CeZrAl, Co90CeZrAl, and CoCeAl.

2.2 Characterization

X-ray diffraction (XRD) analyses were carried out in a Siemens® D5000 instrument with Cu-Kα radiation (2θ range = 10-90 º, step size = 0.03 º, and 500 s of step time). The average crystallite size of Co_3O_4, $d(Co_3O_4)_{XRD}$, was calculated employing Scherrer equation over the (311) diffraction peak of Co_3O_4 XRD pattern at 36,8 º2θ. Additionally, the average crystallite size of metallic species of Co, $d(Co)_{XRD}$, was estimated by means of an empirical approach (Eq.1) described by Schanke et al. [26].

$$d(Co^o)_{XRD} = 0.75 \times d(Co_3O_4) \qquad \text{(Eq.1)}$$

Specific area and textural properties were measured in a Micromeritics® ASAP 2000 unit. Samples were desorbed under vacuum and dried at 250 ºC during 24 h prior to the analysis. Isotherms were generated by adsorption-desorption of N_2 at the liquid nitrogen temperature.

Catalysts reducibility was studied by H_2 temperature programmed reduction (H_2-TPR) using a Micromeritics® Autochem 2910. Calcined samples were treated passing 50 mL/min of 5 vol. % H_2 /Ar, while a heating program from room temperature to 1000 ºC (10 ºC/min) was activated. The H_2-consumption was continuously monitored on a thermal conductivity detector (TCD). In order to calibrate H_2-consumption, Ag_2O powder was used as a standard.

Furthermore, the degree of reduction (DOR) has been also established for all cobalt-containing catalysts using the same apparatus. DOR is a parameter frequently evaluated for cobalt catalysts for FTS to estimate the percentage of reducible species was been reduced after reduction pretreatment (in our case, 16 h at 350 ºC under 200 NmL/min of pure H_2 flow) [27].

Dispersion of metallic cobalt D (%) was estimated using hydrogen static chemisorption on a Micromeritics ASAP 2020C unit. Samples were evacuated at 40°C for 1 h then in situ reduced at 350°C (heating rate: 1°C/ min) for 16 h in a pure H_2 flow. After reduction, samples were evacuated at 330°C for 1 h and then 30 min at 100°C prior to analysis at 35°C. Chemisorption isotherms were extrapolated at zero pressure to determine the amount of adsorbed hydrogen. In all cases, a coverage of two cobalt atoms per molecule of hydrogen was assumed as Bartholomew et al. [28] claim. An average particle size of the Coº species $d(Co)_{H2}$ was established (Eq.2) from chemisorption studies assuming a spherical shape and a density of 14.6 cobalt sites per nm^2 [29].

$$d(Co)_{H2} = \frac{0.96}{D} \cdot DOR \qquad \text{(Eq. 2)}$$

X-ray photoelectron spectra (XPS) of some catalysts were measured using a Leybold-Hereus LHS-10/20 spectrometer with monochromatized Al Kα X-ray radiation, operating at $5 \cdot 10^{-9}$ Torr. Binding energies were corrected according to the C (1s) peak position (284.6 eV) of adventitious carbon. Spectra were analyzed using CasaXPS software and Gaussian-Lorentzian (70:30) curves were used for fitting.

Complementary studies of low-temperature CO adsorption monitored by FTIR were carried out over two selected materials. For that purpose, samples were pressed into self-supporting wafers of ca. 12 mg/cm^2 and activated in situ in a homemade quartz cell, by pretreating under hydrogen at 350 ºC for 1h. Then samples were exposed to small doses of CO up to saturation at 77 K by using a liquid nitrogen-cooled trap and then evacuated. FTIR spectra were recorded with a THERMO NICOLET Avatar 380 FTIR Spectrophotometer, equipped with a DTGS/KBr detector and accumulating 64 scans at a spectral resolution of 4 cm^{-1}. Spectra were collected by using a Nicolet OMNIC software.

2.3 Catalytic activity measurements during the Fischer-Tropsch synthesis

The catalytic performance was evaluated in a Microactivity Reference® unit equipped with a down-flow stainless-steel fixed-bed reactor (internal diameter: 9 mm). The reactor was heated with an electric oven and the temperature was regulated by a cascade control with a sliding thermocouple inside a thermowell placed inside the reactor, and another thermocouple placed in the oven.

During the catalytic performance, a catalyst loading of ca. 1.5 - 2.5 g with particle sizes between 53 – 90 µm was diluted with 8 g of SiC (average pellet size = 53 µm). Prior to FTS experiments, materials were reduced in situ in pure hydrogen during 16 h at 350 ºC (1 ºC/min). Subsequently, the fixed-bed temperature was set at 210ºC ± 2ºC, and then, the reactor was pressurized with He (20 bar). All catalytic tests were carried out in four stages along 100 h total time on steam, in order to evaluate the total conversion, the selectivity and the effect of including water in the feed-stream respectively:

- (Stage 1) Catalytic activity measurement at constant space velocity: firstly catalysts were tested under the same space velocity (syngas total flow: 15 Nl/h; [H_2/CO molar ratio = 2.1]).
- (Stage 2) Space velocity modification until achieving a constant CO conversion of 35% in all catalytic systems in order to compare selectivity at isoconversion.
- (Stage 3) Inclusion of water in the feed-stream: keeping the space velocity of Stage 2 (isoconversion of CO in every system) but including a 20 Vol.% of $H_2O_{(g)}$.
- (Stage 4) Substitution of water from the feed-stream by Helium: keeping the space velocity of Stages 2-3, and replacing water by a 20 Vol.% of He.

Two consecutive traps were installed out the stream to separate liquid products fraction: Heavy long-chain hydrocarbons were caught in a first hot trap (at 120 ºC), while water and lighter hydrocarbons were condensed in the second one at room temperature. Gaseous products were depressurized and then analyzed in a gas chromatograph (GC) Agilent 6890, equipped with a Carbosieve II packed column, a thermal conductivity detector (TCD) and a flame ionization detector (FID). CO, CO_2 and C_1-C_4 hydrocarbons products were separated by means of an alumina-plot column and then individually quantified.

Selectivity to CO_2 was calculated according to Eq.3:

$$SCO_2 = \frac{moles\ of\ CO_2\ produced}{moles\ CO\ reacted} \cdot 100 \qquad \text{(Eq.3)}$$

In analogous form, selectivity to hydrocarbons with the same number of carbon atoms, C_i with i= 1, 2, 3, 4, was estimated from the atomic carbon balance following Eq.4.

$$SC_i = \frac{\sum moles\ of\ hydrocarbons\ with\ i\ atoms\ of\ C\ produced * i}{moles\ CO\ reacted} \cdot 100 \qquad \text{(Eq.4)}$$

Since hydrocarbon with 5 or more carbon atoms (C5+) are not detected by our analytical system, the selectivity towards these higher hydrocarbon (S_{C5+}) was calculated closing the carbon balance, according to Eq.5:

$$SC5+ = 100 - (SC_1 + SC_2 + SC_3 + SC_4 + SCO_2) \qquad \text{(Eq.5)}$$

The olefin to paraffin molar ratio (o/p) for molecules with 2, 3 and 4 carbons (C_2, C_3 and C_4 respectively) is estimated as the total amount of olefins detected (moles) divided by the total amount of paraffin detected (moles) with equal number of carbons atoms.

3. Results and discussion

3.1. Physicochemical properties of the prepared materials

All studied physicochemical properties are summarized in Table 1, including support and catalyst textural and structural properties as well as particle sizes and dispersion of cobalt phase.

Supports and catalysts textural properties are similar to those of the parent alumina, as expected [30]. Solids exhibited IV type isotherms and H3 type hysteresis loop (not shown), commonly related to slit-like shape pores.

The calcination of fresh alumina decreased its surface area that agrees with the thermal contraction observed by Busca et al. [31]. These authors associate a specific area and a pore volume decreasing of γ-Al_2O_3 with the destabilization of its strong faulting spinel-like structure, as occurs during the transformation between different phases of alumina (γ,δ,η-Al_2O_3).

Moreover lightly modifications of BET surface area values were obtained after alumina modification with oxide promoters. In fact, supports BET surface area are relatively close to each other. Nevertheless, it is observable that surface area slightly increases with Zr- loading.

Comparison between catalysts and supports average pore diameters shown that catalysts pore volume are by 27-35% below from those corresponding supports. That contraction is related to the expected strong interaction between cobalt and the support. Moreover, Ce-presence within the catalysts formulation seems to favor these textural values decrease (Table 1).

XRD patterns of prepared materials are presented in Figure 1. Firstly, non-modified alumina pattern (Al sample) corresponds to that of the spinel-like γ-Al_2O_3 (JCPDS: 29-0063) with spatial group Fd3m. As for 50CeZrAl, 90CeZrAl and CeAl solids, these present main reflections of the γ-Al_2O_3 pattern along with those of the fluorite-like structure of ceria (JCPDS: 34-0394). However, in case of 50CeZrAl and 90CeZrAl solids, a shift of these reflections is caused by the ceria structure. Since a shift towards higher 2θ values is observed, a solid solution formation between CeO_2 and ZrO_2 phases is proposed. Thus, the inclusion of Zr into ceria framework results in the evolution of $Ce_xZr_{x-1}O_2$ phase as well as in a decreasing of the oxide promoter lattice parameter from 5.400 Å in CeAl to 5.351Å in 50CeZrAl (See Table 1).

Regarding ZrAl and 10CeZrAl solids, the presence of oxide promoter crystalline phases is only discernible by the evolution of a broad reflection between 25-35 º 2θ. In this zone, the occurrence of the (111) crystallographic planes reflections of tetragonal ZrO_2 phase or that of the cubic CeO_2 is expected. However, our samples reveal a remarkable broadness of the cited reflection and this may indicate the overlapping of some structural lines. For instance, a Ce/Zr solid solution formation in the 10CeZrAl solid throughout the inclusion of cerium cations within zirconia framework could result in such broad XRD signals. Or the evolution of Zr-containing phases with a low crystallographic domain, which results in a highly disordered oxide phase over alumina surface. Similar behavior has been described by Souza et al. [20] in a zirconia doped alumina study. They have concluded a formation of highly dispersed ZrO_2 crystals over alumina occurs whether the oxide loading is below 17.5 wt. %, which demonstrates a strong interaction between these two phases. In our case, a strong interaction between the Zr-rich oxide promoters and alumina is revealed not only because a low crystalline domain of the Zr-containing phases in ZrAl and 10CeZrAl solids but also because the previously observed support surface area promotion with increasing Zr concentration (see Table 1).

Regarding catalysts XRD patterns (Figure 1C), main reflections of the corresponding supports are still observable. Additionally, diffraction lines associated to Co_3O_4 cubic phase (JCPDS 42-1467) are also noticeable, although the presence of $CoAl_2O_4$ should not be discarded since both XRD pattern may be indistinguishable at this experimental conditions. Applying Scherrer equation to the (311) reflection of Co_3O_4 phase, the average size of Co_3O_4 crystallites ($d(Co_3O_4)_{XRD}$) were estimated (Table 1). Assuming the empirical approach described in [26] and taking into account the corresponding crystallographic parameter an average size of metallic cobalt nanoparticles, $d(Co)_{XRD}$, could be estimated (seen in Table 1). These results demonstrate particle size of cobalt species (metallic or oxides) seem to decrease the amount of Zr, which would mean that the amount of Zr directly influences cobalt species dispersion. Despite lightly differences in cobalt species particle size is evidenced the effect of Zr over the cobalt dispersion could be produced by the observed improvement of textural properties. This superior BET surface area, pore volume and average pore sizes (Table 1) would result in an improved surface for smaller cobalt species formation. Such statement can be reinforced through XPS experiments carried out in CoAl and CoZrAl catalysts as presented in Figure 2.

Regarding spectra of the Al(2p) core level, a shift of 0.5 eV is exhibited confirming environment alterations of aluminum species surface due to interactions with zirconia phases. Such interaction is also modifying cobalt species electronic environment as confirmed throughout the observed shift of $2p_{1/2}$ and $2p_{3/2}$ corresponding to Co(2p) peaks of the core level spectra. Moreover, the calculation of the Co/(Zr+Al) molar ratio included in Figure 2, suggests a slightly superior surface concentration of cobalt species in the CoZrAl catalyst. Thus, higher cobalt surface concentration in Zr promoted catalyst than that of CoAl may sustain the effect of Zr promotion is related to easily reducible cobalt species formation onto catalyst surface.

The dispersion of cobalt species was measured by means of H_2-chemisorption experiments and results are presented in Table 1. In general, chemisorption values are shown larger metallic cobalt particle sizes than those determined with XRD data and there are no clear trends between the metallic cobalt species size or their dispersion and supports chemical composition. This discrepancy between results obtained by XRD and chemisorption is probably due to a sintering of cobalt species during the reduction process at 350 ºC, which is

not applied during the XRD but prior to chemisorption experiments [32-33]. It has to be mentioned that catalyst reduction atmosphere during chemisorption experiments is simulating activation conditions used prior to catalytic activity measurements. For that reason, chemisorption results are expected closer to the real nature of active cobalt species prior to FTS. Although considering our results, there is not a specific trend between the support chemical composition and cobalt species dispersion.

Nevertheless, our results are not in agreement with those reported by Rane et al. [33] since these authors have confirmed a linear correlation between values of $d(Co)_{XRD}$ and $d(Co)_{H}$ obtained by similar Co/Al_2O_3 catalyst. In their case, cobalt has been dispersed over bare alumina without any promoter but the presence of promoters with a reducible character may interfere in our case. Consequently, hydrogen consumption is probably overestimated depending on the amount and availability of reducible promoter oxide phase particularly ceria. Actually, Damyanova et al. [34] have reported H_2-chemisorption over ceria species in alumina doped with 12 wt.% of CeO_2 below the temperature of the reduction processes (<350 ºC). And even for zirconia, which is considered a non-reducible phase has demonstrated an induction of cobalt species dispersion in $Co\text{-}ZrO_2$ catalysts as reported Enache et al. [16].

Regarding catalysts reducibility, TPR profiles are presented in Figure 3. According to the literature [6], Co/Al_2O_3 catalysts present TPR profile with two differentiated reducibility regions. In our samples, these two regions (labeled as Zone I and Zone II) have been also observed.

Below 500 º C (Zone I), the H_2 consumption is related to the reduction of a bulk-like Co_3O_4 spinel, while cobalt species strongly bounded to alumina lattice (forming cobalt aluminates or not) are reduced at higher temperatures (between 500-1000 ºC, Zone II). Similarly, Chu et al. [35] are describing same behavior in Co/Al_2O_3 catalysts.

The Zone I correspond to 200-500 ºC range which has been associated with non-stoichiometric sequenced steps of Co_3O_4 reduction to Co^0 ($Co^{+3} \rightarrow Co^{+2} \rightarrow Co^0$) [6]. Accordingly, a bimodal behavior is observed in our catalysts as expected. However, this bimodal profile presents some differences among our materials. For instance, the inclusion of both Ce and Zr promoters induce the slight reduction peak to shift towards lower

temperatures. Furthermore, the relative intensity of the Zone I first peak respect to the second one is observed superior in Zr-rich catalysts (CoZrAl and Co10CeZrAl).

Different performances observed in Zone I demonstrate that interactions between Co species and support depend on support formulation. In fact, Co10CeZrAl profile suggests the highest reducibility promotion (highest shift of the Zone I reduction peaks towards lower temperatures). Since a greater inhibition of the Co-Al interaction is resulting in more available number cobalt active species.

According to the literature [13], no reduction peaks should be expected due to the modification of alumina with zirconia. Therefore, small crystals of zirconia observed in XRD experiments may be homogeneously dispersed over alumina surface inhibiting cobalt diffusion into alumina matrix thus favoring the availability of cobalt reducible species after calcination [36].

However other authors are not discarding the H_2-chemisorption over ZrO_2 phases that may result in an increase of cobalt active species in Zr modified alumina due to spillover processes [16]. In this sense, analogous results were found by Kraum et al. [37] using bulk ZrO_2 and CeO_2 as support for Co-based catalysts. These authors observed a higher promoting effect of zirconia compared with that of ceria-based on the H_2-consumption during the reduction of cobalt species at low temperatures (<400 ºC).

Concerning the broad hydrogen consumption from 500 to 1000 ºC (zone II), this is produced by hard to reduce cobalt- aluminum oxide species formed by diffusion of cobalt ions into alumina during the calcination step. Only using noble metal as promoters (e.g. Pt, Re) is possible to shift these reduction events to lower temperatures [12, 36]. Therefore, assuming that only Co^{+2} species are reduced in the Zone II [27, 35], the $CoAl_2O_4/Co_3O_4$ molar ratio could be estimated from the ratio between hydrogen consumptions in zones I and II (see Table 1). On one hand, obtained $CoAl_2O_4/Co_3O_4$ values demonstrate those promoters presence always result in a superior amount of easily reducible cobalt species. On the other hand, no big differences in $CoAl_2O_4/Co_3O_4$ values corresponding to promoted catalysts have been observed. Although these values have to be carefully considered (above all Ce-rich solids) since hydrogen consumption produced by the reducible species of the promoter has not been considered. In summary, the reducibility promotion depends on the combination of

two variable factors: 1) the inclusion of cerium reducible species and 2) H_2 -spillover processes induced by promoter oxides towards cobalt species.

Additionally, DOR values (see Table 1) can be considered as an estimation of cobalt active species available before FTS. Narrow differences in DOR (%) values are found among the catalysts, suggesting the analogous amount of active cobalt species in all catalyst. Nevertheless, CoAl and Zr-rich catalyst present higher DOR values than those solids with higher Ce- loadings (except to Co90CeZrAl). Consequently, this behavior seems suggest that the promoter effect over reducibility is closely associated to H_2-spillover rather than to the inclusion of a reducible phase. This statement is confirmed by the fact that DOR values overestimation in Ce-rich catalyst is due to the contribution of cerium reducible species.

3.2. FTS catalytic performance and correlations with catalyst physicochemical properties

The results of the catalytic activity measurements carried out in four stages over the prepared catalysts are presented below:

- *Stage 1:* Primarily, the catalytic activity of all prepared catalysts was compared under same experimental conditions and results are presented in Figure 4. Turnover frequencies, (TOF), were calculated using the following equation, Eq.6.

$$TOF\ (s^{-1}) = \frac{CO\ consumption}{Availiable\ Co\ moles} \qquad \text{(Eq.6)}$$

Where:
CO consumption = CO moles converted per second
Available Co moles = loading of Co moles * Dispersion/100

Highest TOF value means superior catalytic activity. CoZrAl followed by the CoAl are then the most active catalysts. Concerning the Ce-rich catalysts, they present the lower catalytic performance ordered as: Co10CeZrAl > Co90CeZrAl > Co50CeZrAl > CoCeAl. Therefore, it is clear that Ce-inclusion results in a catalytic activity detrimental. This behavior demonstrates that the availability of easily reducible cobalt species, enhanced by the oxide promoters is determinant for increasing the catalytic activity by a superior availability of

active sites for FTS. Consequently, zirconia as a promoter would be acting as an inhibitor of a strong metal-support interaction (SMSI) between Co and alumina [6].

This is in agreement with the currently observed superior DOR values in Zr-rich systems. On the contrary, the catalytic performance decreasing with Ce-inclusion indicates that the interaction between cobalt and cerium is unproductive. This would suggest that CeO_2 as promoter generates instead of inhibiting Co-Al SMSI making Co particles even less active during the FTS than those of Co/Al_2O_3 catalyst. Therefore, although Ce-rich catalysts present reducibility modifications respected to those without cerium, these alterations do not positively contribute to the availability of active species of Co. Rohr et al. [17] have found a similar improvement in zirconia modified cobalt alumina catalysts studied with Steady State Isotopic Transient Kinetic Analysis (SSITKA). These authors have attributed to zirconia samples an unexpected enhancement on surface coverage of reactive intermediates, but any changes in the intrinsic activity. In agreement with this, Jongsomjit et al. [13] have proposed that the principal reason for the promotion with Zr is the alumina stabilization by blocking its defect sites. This is hindering partially cobalt-aluminate formation. In addition, the presence of Zr also minimizes the steam impact on the modified alumina surface properties, thereby decreasing the easiness of Co reaction with the alumina. This is in agreement with the observed lower $CoAl_2O_4/Co_3O_4$ ratios (see Table 1) suggesting less formation of cobalt aluminates. Apart from this, Enache et al [16] are also claiming the relevance of the surface promotion on the FTS catalytic performance, which is the case of our Zr-rich catalysts that present superior BET surface areas (Table 1).

- ***Stage 2:*** Catalytic performance under isoconversion conditions generated results presented in Table 2, including values of selectivities towards methane (SCH_4), hydrocarbons with more than five carbons (SC_{5+}), and CO_2 (SCO_2), as well as the olefin to paraffin molar ratio (o/p) for molecules with 2, 3 and 4 carbons (C_2, C_3 and C_4 respectively).

Under isoconversion conditions, selectivity values exhibit a slightly superior ability of the CoZrAl system to produce long hydrocarbons (SC_{5+}) rather than CH_4 or CO_2 in agreement with other reports devoted to study similar catalysts for FTS [10,13,16-18]. On the contrary, Ce inclusion in catalysts formulation generates the opposite behavior, which in principle is in disagreement with some reports about FTS on Ce promoted cobalt catalysts where this promoter enhance activity due to its widely demonstrated oxygen mobility[38-40].

The o/p ratio is closely related with SC_{5+} values according to Rane et al. [33]. They have observed olefins readsorption leads to the hydrocarbon chain growing. This could agree with our results although narrow differences are observed in the o/p ratio values. These are lower for Zr-rich systems, which means a promotion of larger chains formation. In fact, Iglesia et al. [41] have proposed that readsorption of olefins is enhanced with increasing availability of cobalt active sites, which is the case of Zr-promoted systems where zirconia is the main framework of the promoter oxide, according to the XRD and XPS results presented above.

In literature, proper interaction between Co-Zr-Al phases in CoZrAl catalysts was recently explained by Johnson et al. [42] as a consequence of a Co-Zr monolayer formation which enhances both CO adsorption constant and CO consumption rate coefficient, especially for Co/Zr ratios close to 1. However, supports chemical composition particularly systems proposed in the present work seems to be a driving force that may modify the pathway of the global process. Regarding effects of support chemical composition, Maitlis et al. [3] have proposed that FTS mechanism is affected by polarizing surfaces. Then, considering the FTS monomer as an electrophilic specie, the CO molecules activation could be carried out by polarizing surfaces such as the cobalt-promoter oxide interphase, where C-terminations are bonded to cobalt particles, while O-terminations are linked to acids sites of the promoter oxide. These authors also remarked that the success of a promoter oxide can be associated with its acidic properties, specifically Lewis acidity. Although bare alumina is well known to have a strong intrinsic Lewis acidity, such modification due to species capable to provide Lewis acidic properties would result, in the enhancement of the catalytic performance. From our catalytic activity measurements, this could be a promoter role revealed in zirconia rather than ceria samples [6].

The shown sequence of the catalytic activity performance is in good agreement with the classification proposed by Daturi et al. [43] in a study of acidic properties of zirconia, ceria and Ce-Zr mixed oxides. By means of CO and pyridine adsorption experiments, these authors have demonstrated that Lewis acidity of surface Zr^{4+} species is higher than that of surface Ce^{+4} species. An intermediate situation was observed for the Ce-Zr mixed oxides. Thus the acidity order decreases as follows: $ZrO_2 > Ce_xZr_{x-1}O_2 > CeO_2$. In agreement with this, Prieto et al. [14] have described a volcano dependence of the oxide promoter acidity with both the activity and the selectivity during the FTS reaction.

Considering later evidences about the key role of support acidity properties in FTS activity, a detailed analysis is required to elucidate the influence of zirconia and ceria promotion on the alumina acid sites nature (Lewis or Brønsted), concentration and strength and its relationship with FTS performance. In order to provide some preliminary insights, we have been performed a FTIR study of the CO adsorption at 77 K (as probe molecule) on our two extreme case supports (CeAl and ZrAl). The IR spectra in the OH and CO stretching regions recorded for increasing amounts of adsorbed CO at low temperature (77 K) on both solids are presented in Figures 5 and 6.

In the case of the ZrAl support (Figure 5) the bands in the OH stretching region at 3675 and 3550 cm^{-1} remained unaffected after CO adsorption indicating that these hydroxyl groups are either not accessible or not acidic. Only the bibridged hydroxyls (3735 cm^{-1}) seems to be perturbed by the interaction with the CO molecule generating a new broadband centered at 3615 cm^{-1} in which a $\Delta\nu$(OH) shift of 120 cm^{-1} is indicative of the presence of relatively weak Brønsted acid sites in comparison with pure alumina (155 cm^{-1}) [44-45].

The 3900–3300 cm^{-1} spectral range of the CeAl support (Figure 6) is dominated by the progressive disappearance of the bands located at 3768, 3746 and 3723 cm^{-1} while an intense and broadband centered at 3600 cm^{-1} is developed suggesting the formation of OH groups H-bonded to CO. A minor weaker feature at ca. 3751 cm^{-1} is also discernible and can be ascribed to a weak interaction of CO with terminal OH groups of tetrahedral aluminum centres (Al IV). The broadband at 3600 cm^{-1} can be assigned to the ν(OH) vibration of the 3723 - 3746 cm^{-1} bibridged hydroxyls groups H-bonded to CO [46]. The frequency shift of the 3723 cm^{-1} band upon CO adsorption can be estimated to ca. 123 cm^{-1}, suggesting that the corresponding hydroxyl species are weak Brønsted acid sites, similar to those presented at the surface of ZrO_2/Al_2O_3. The most significant difference arises in the ν(CO) region in which the CO adsorption resulted in the appearance of a complex set of bands. Bands positions were determined using bands second derivatives of saturation spectra. In this manner, we identified four different sites of CO adsorption at 2190, 2179, 2165 and 2146 cm^{-1}. Bands at 2190 and 2165 cm^{-1} can be assigned to Al^{3+}-CO and Al-OH-CO species, respectively [47] while the bands at 2179 and 2146 cm^{-1} can be attributed to Ce^{4+} and Ce^{3+} coordinately unsaturated sites, respectively [44-45, 48-51]. Furthermore, the presence of one a band to 2124 cm^{-1} is typical of reduced ceria [47]. For the smallest CO doses, the band at 2179 cm^{-1} band appeared

firstly, and then gradually disappear accompanied by the development of the band at 2146 cm^{-1}. This indicates that CO is reducing the Ce^{4+} to Ce^{3+} during the adsorption.

According to this preliminary studies of ZrAl and CeAl supports by FTIR, the presence of ceria seems to increase support Lewis acidity, while zirconia in one hand seems to partially inhibit the Lewis acidity and, on the other hand, it is enhancing some Brønsted acid sites. These observations are clearly in disagreement with the previously cited about the role of zirconia as a promoter of Al_2O_3Lewis acidity rather than an inhibitor of such feature [43]. Despite this fact, our spectroscopic study should be complemented in order to establish more clear conclusions about the influence of acidic properties. These preliminary results consider the apparent inhibition of alumina acidity by zirconia, probably by a physical blockage of alumina surface acidic sites through a zirconia phase coverage.

If solids chemical composition is analyzed, both materials present a loading of 20 wt.% of promoter oxide. This means that the ZrAl solid has a superior number of moles of zirconia (~28% more) than ceria moles of CeAl solid. Despite this, the XRD patterns demonstrated that the crystalline domain of zirconia is lower than that of ceria, even though zirconia is highly concentrated. Therefore, the strong interaction between zirconia and alumina, that produce a high dispersion of this promoter, is also confirmed through the blockage of acid sites, while ceria allows an easier access to intrinsic alumina acidic sites.

In this sense, although the ZrAl system presents the highest catalytic performance among the studied solids, this will be probably enhanced if the promotion of the acidic properties of the alumina is carried out. For this purpose, the reformulation of a more suitable chemical content of zirconia is required, but always inhibiting, as much as possible, the Co-Al_2O_3 interaction.

- *Stages 3 and 4*: Results corresponding to the presence of water within the feed-stream during FTS are presented in Figure 7. Obtained data has been labeled as wet or dry in Figure 7, indicating the presence or absence of water, respectively, and includes the CO consumption rate, selectivities towards methane production (SCH_4), production of hydrocarbons with more than five carbons (SC_{5+}), and CO_2 production (SCO_2), as well as the olefin to paraffin molar ratio (o/p) for molecules with 2, 3 and 4 carbons (C_2, C_3 and C_4 respectively).

A general comparison of CO consumption rate during both periods (Figure 7A) evidences that CoAl catalyst presents the highest performance, followed by Zr-rich catalysts and finally those materials with Ce, where the yield is decreasing as the loading of Ce increases. Furthermore, comparing all catalyst yields, the performance is higher for CoAl catalyst as well as for the CoZrAl and Co10CeZrAl in the wet period. This result could agree with the proposed autocatalytic water effect described by Iglesia et al. [8]. These authors have considered a reaction-transport model where water allows enhancing the accessibility of CO and H_2 molecules to the porous support structure, resulting in an enhancement of CO consumption rate and SC_{5+} selectivity. Nevertheless, individual yields of Co50CeZrAl, Co90CeZrAl and CoCeAl catalysts have been observed the opposite behavior during the dry period. These are slightly above of those of wet period. Therefore the water autocatalytic effect seems not happening in this case. Probably as a consequence of Ce-presence since this oxide has demonstrated strong interaction with water molecules. Such interaction has been attributed to the affinity of ceria oxygen vacancies to water molecules that probably inhibits the autocatalytic effect of water and resulting in a decrement of activity in FTS.

Another relevant aspect described in the water autocatalytic effect cited above [8] is that the decreasing of transport restrictions results in an olefin production enhancement. Since the readsorption of the produced hydrocarbons is favored by the contact time. This could agree with our results since SC5+ is superior during the wet period in all cases, while SCH_4 is lowered (see Figures 7A and 7B). Moreover, SC_{5+} values decrease with the inclusion of cerium, while the SCH_4 exhibits the opposite trend. Concerning SCO_2 values, these are higher in wet period for all cases. Such SCO_2 values increase with Ce loading in the catalysts. Therefore, the decreasing of SC5+ may agree with the promotion of side reactions enhancing CO_2 production.

Although further experiments are required to determine FTS mechanism, our C2, C3 and C4 o/p ratio values could give some interesting clues on it. These values are superior for the wet period in all cases (Figures E-G). All of them decrease as the proportion of Ce increases. However the presence of water seems to exert a leveling effect [52] over catalysts acidic properties, thus balancing o/p ratio values in the case of CoAl, CoZrAl Co10CeZrAl and Co50CeZrAl catalysts.

4. Conclusions

The synthesis of cobalt catalysts supported over modified alumina has been successfully carried out using Zr and/or Ce as oxide promoters. Characterization of the obtained materials revealed that the interaction between the oxide promoter and alumina is resulting in a protection of the alumina main textural properties during calcination step. This stabilization effect is evidenced in Zr-rich solids, where a strong interaction between Zr and Al was demonstrated. Additionally, the formation of cobalt aluminates considered as less active species for FTS is inhibited by the inclusion of both oxide studied promoters, although it is more evident in the case of Zr. Furthermore, cobalt reducibility at low temperatures is also altered and, promoted by the presence of the oxide promoters in principle.

Concerning catalytic activity measurements, highest performances in FTS is observed for CoZrAl catalyst followed by Co10CeZrAl, while the solids with superior loadings of ceria exhibited a decrease of their catalytic activity.

Under isoconversion conditions, catalysts with higher loadings of Ce presented lower selectivities towards long-chain hydrocarbons formations, as well as an enhancement of the selectivity towards CH_4 and CO_2.

Regarding the analysis of the effect of water presence, an autocatalytic effect seemed to be noticeable, since selectivity towards long hydrocarbons formation was improved in all cases, especially for those Zr-rich systems. In addition, comparing the different o/p ratios, a clear modification of the trend was observed with the inclusion of water, demonstrating the influence of water over the FTS pathway. Once again, systems promoted with high amounts of Zr presented higher performances.

Catalytic activity and characterization results are revealing the importance of the inhibition of SMSI between Co-Al species that is favored in Zr-rich solids. It appeared to be more significant than the enhancement of reducibility. In addition, preliminary results about the acidic properties are showing differences between the promotion by ceria and zirconia. However, catalysts formulation should be optimized in order to enhance the acidic properties.

5. Acknowledgements

Financial support for this work has been obtained from the Spanish Ministerio de Economía y Competitividad (MINECO) (ENE2012-374301-C03-01 and ENE2015-66975-C3-2-R),

cofinanced by FEDER funds from the European Union. Victoria Garcilaso acknowledges MINECO by their FPI fellowships (BES-2013-062806) and (EEBB- I- 15-09959).

6. References

[1] S.S. Ail, S. Dasappa, Renew. Sustain. Energy Rev. 58 (2016) 267-286

[2] J. Rostrup-Nielsen, L.J. Christiansen, Concepts Syngas Manufacture, Catalytic Science Series Vol.10, (2011)

[3] P.M. Maitlis, V. Zanotti, Chem. Commun. (2009) 1619-1634

[4] M.E. Dry, Catal. Today 71 (2002) 227-241

[5] M.A. Vannice, J. Catal. 50 (1977) 228-236

[6] A.Y. Khodakov, W. Chu, P. Fongarland, Am. Chem. Soc. 107 (2007) 1692-1744

[7] H. Schulz, Appl. Catal., A 186 (1999) 3-12

[8] E. Iglesia, Appl. Catal., A 161 (1997) 59-78

[9] N.E. Tsakoumis, M. Rønning, Ø. Borg, E. Rytter, A. Holmen, Catal. Today 154 (2010) 162-182

[10] E. Rytter, A. Holmen, Catalysts 5 (2015) 478-499

[11] E. Iglesia, S.L. Soled, R. A. Fiato, G.H. Via, J. Catal. 143 (1993) 345-368

[12] D. Nabaho, J.W.H. Niemantsverdriet, M. Claeys, E. Van Steen, Catal. Today 261 (2016) 17-27

[13] B. Jongsomjit, J. Panpranot, J.G. Goodwin, J. Catal. 215 (2003) 66-77

[14] G. Prieto, M.I.S. De Mello, P. Concepción, R. Murciano, S.B.C. Pergher, A. Martínez, ACS Catal. 5 (2015) 3323-3335

[15] K. Shimura, T. Miyazawa, T. Hanaoka, S. Hirata, Appl. Catal., A 494 (2015) 1-11

[16] D.I. Enache, M. Roy-Auberger, R. Revel, Appl. Catal., A 268 (2004) 51–60

[17] F. Rohr, O.A. Lindvåg, A. Holmen, E.A. Blekkan, Catal. Today 58 (2000) 247-254

[18] Y. Zhang, H. Xiong, K. Liew, J. Li, J. Mol. Catal. A: Chem. 237 (2005) 172-180

[19] W. Ma, G. Jacobs, P. Gao, T. Jermwongratanachai, W.D. Shafer, V. Ramana, R. Pendyala, C.H. Yen, J.L.S. Klettlinger, B.H. Davis, Appl. Catal., A 475 (2014) 314-324

[20] M.M.V.M. Souza, D. A G. Aranda, C. a C. Pérez, M. Schmal, Phys. Status Solidi A 187 (2001) 297-303

[21] F. Pardo-Tarifa, S. Cabrera, M. Sanchez-Dominguez, M. Boutonnet, Int. J. Hydrogen Energy 42 (2017) 9754-9765

[22] S. Haibo, S. Shikong, Chin. J. Catal. 27 (2006) 1096-1100

[23] B. Sarup, B.W. Wojciechowski, Can. J. Chem. Eng. 67 (1989) 62-74

[24] O.H. Laguna, A. Pérez, M. A. Centeno, J. A. Odriozola, Appl. Catal., B 176-177 (2015) 385-395

[25] M. Fernández-García, A. Martínez-Arias, A. Iglesias-Juez, C. Belver, A.B. Hungría, J.C. Conesa, J. Soria, J. Catal. 194 (2000) 385-392

[26] D. Schanke, S. Vada, E.A. Blekkan, A.M. Hilmen, A. Hoff, A. Holmen, J. Catal. 156 (1995) 85-95

[27] Ø. Borg, R. Magnus, S. SØlvi, Van B. Wouter, H. Anders, Stud. Surf. Sci. Catal. 163 (2007) 255-272

[28] R.C. Reuel, C.H. Bartholomew, J. Catal. 77 (1984) 63-77

[29] C.H. Bartholomew, R.J. Farrauto RJ (2010) Fundamentals of industrial catalytic processes, 2nd edn. Wiley, Hoboken

[30] P.S. Santos, H.S. Santos, S.P. Toledo, J.Mater. Res. 3 (2000) 104-114

[31] G. Busca, Catal. Today 226 (2014) 2-13

[32] M.A. Arribas, G. Prieto, Appl. Catal., A 367 (2009) 146-156

[33] S. Rane, O. Borg, E. Rytter, A. Holmen, Appl. Catal., A 437–438 (2012) 10-17

[34] S. Damyanova, J.M. Bueno, Appl. Catal., A 253 (2003) 135-150

[35] W. Chu, P. A. Chernavskii, L. Gengembre, G. A. Pankina, P. Fongarland, A.Y. Khodakov, J. Catal. 252 (2007) 215-230

[36] A. M. Hilmen, D. Schanke, A. Holmen, Catal. Letters 38 (1996) 143–147

[37] M. Kraum, M. Baerns, Appl. Catal., A 186 (1999) 189–200

[38] B. Ernst, L. Hilaire, A Kiennemann, Catal. Today 50 (1999) 413-427

[39] X. Dai, C. Yu, R. Li, H. Shi, S. Shen, Chinese J. Catal. 27 (2006) 904-913

[40] J. Barrault, A. Guilleminot, J.C. Achard, V. Paul-Boncour, A. Percheron-Guegan, Appl. Catal. 21 (1986) 307-312

[41] E. Iglesia, S.L. Soled, R.A. Fiato, J. Catal. 137 (1992) 212-224

[42] G.R. Johnson, A.T. Bell, ACS Catal. 6 (2016) 100-114

[43] M. Daturi; C. Binet, J.C Lavalley, A. Galtayries, R. Sporken, Phys. Chem. Chem Phys. 1 (1999) 5717–5724

[44] L. Oliviero, A. Vimont, J. Lavalley, F.R. Sarria, M. Gaillard, F. Maugé, Phys. Chem. Chem. Phys. 7 (2005) 1861-1869

[45] C. Morterra, G. Cerrato, S. Di Ciero, Appl. Surf. Sci. 126 (1998) 107-128

[46] C. Morterraj, V. Bolis, G. Magnacca, J. Chem. Soc., Faraday Trans., 92 (1996) 1991-1999

[47] M.A. Centeno, K. Hadjiivanov, T. Venkov, H. Klimev, J.A. Odriozola, J. Mol. Catal. A: Chem. 252 (2006) 142-149

[48] A.A. Tsyganenko, V.N. Filimonov, Spectrosc. Lett. 5 (1972) 477-487

[49] O. Cairon, T. Chevreau, J.-C. Lavalley, J. Chem. Soc., Faraday Trans., 94 (1998) 3039-3047

[50] X. Chen, G. Clet, K. Thomas, M. Houalla, J. Catal. 273 (2010) 236-244

[51] K. Hadjiivanov, J. Lavalley, Catal. Commun. 2 (2001) 129-133

[52] F.Atkins, P.W. Overton, T.L.Rourke, J. P. Weller, M. T. Armstrong, Shriver and Atkins' Inorganic Chemistry, Oxford University Press, 2010

Tables

Table 1. Physicochemical properties of the prepared materials

Prepared solids		BET Surface Area (m^2/g)	Pore Volume (cm^3/g)	Average pore diameter (nm)	$d(Al_2O_3)_{XRD}$ (nm)	Cell parameter (a) ($Ce_xZr_{x-1}O_2$) (Å)	$d(Co_3O_4)_{XRD}$ (nm)	$d(Co)_{XRD}$ (nm)	$d(Co)_H$ (nm)	Dispersion (%)	DOR (%)	$CoAl_2O_4$ / Co_3O_4 ratio
Supports	Al fresh	173	0.53	9.4	5	--	--	--	--	--	--	--
	Al	164	0.48	8.4	5	-	--	--	--	--	--	--
	ZrAl	180	0.44	7.1	5	5.099	--	--	--	--	--	--
	10CeZrAl	176	0.49	7.8	5	5.232	--	--	--	--	--	--
	50CeZrAl	175	0.44	7.5	5	5.351	--	--	--	--	--	--
	90CeZrAl	170	0.44	7.9	4	5.389	--	--	--	--	--	--
	CeAl	164	0.37	7.0	4	5.400	--	--	--	--	--	--
Catalysts	CoAl	139	0.35	8.1	--	--	9	7	13	3.1	39	1.6
	CoZrAl	147	0.32	6.8	--	--	9	7	12	3.3	40	1.1
	Co10CeZrAl	156	0.34	7.2	--	--	10	8	15	2.7	41	1.1
	Co50CeZrAl	138	0.32	7.5	--	--	10	8	9	3.6	35	1.1
	Co90CeZrAl	133	0.29	7.1	--	--	12	9	16	2.5	42	1.3
	CoCeAl	121	0.24	6.5	--	--	12	9	9	3.7	35	1.5

Table 2. Catalytic activity results during the Stage 2

Catalysts	SCH_4	SC_{5+}	SCO_2	o/p C_2	o/p C_3	o/p C_4

	(%)	(%)	(%)			
CoAl	8.8	82.2	0.4	0.2	2.8	1.8
CoZrAl	8.4	82.9	0.3	0.2	3.0	2.0
Co10CeZrAl	9.3	81.7	0.4	0.2	3.0	2.0
Co50CeZrAl	10.0	81.0	0.8	0.3	2.9	2.0
Co90CeZrAl	9.9	80.0	1.0	0.3	3.0	2.1
CoCeAl	9.5	78.2	1.3	0.5	3.6	2.4

Figure captions

Figure 1. XRD patterns of the prepared solids: A) calcined supports; B) zoom in the 20-40 $^{o}2\theta$ range of the calcined supports; C) calcined catalysts

Figure 2. XPS spectra of the Al(2p) and Co(2p) core-levels of the CoAl and CoZrAl catalysts

Figure 3. TPR profiles of the calcined catalysts: A) general TPR profiles; B) Extended view of the TPR profiles Zone I

Figure 4. Catalytic activity during the Stage 1 (Comparison of the catalysts under the same space velocity)

Figure 5. FTIR difference spectra of ZrAl support after the adsorption of small doses of CO in the v(OH) region (A) and the v(CO) region

Figure 6. FTIR difference spectra of CeAl support after the adsorption of small doses of CO (OH) region (A) and the v(CO) regions. The inset shows the heat adsorption estimated for the adsorption of CO on the different Lewis acid sites

Figure 7. Effect of the inclusion of water within the feed-stream during the FTS. A) CO consumption rate; B) Selectivity to CH_4; C) Selectivity to C5+; D) Selectivity to CO_2; E) o/p ratio in C2; F) o/p ratio in C3; G) o/p ratio in C4

Figures

Figure 1. XRD patterns of the prepared solids: A) calcined supports; B) zoom in the 20-40 º2θ range of the calcined supports; C) calcined catalysts

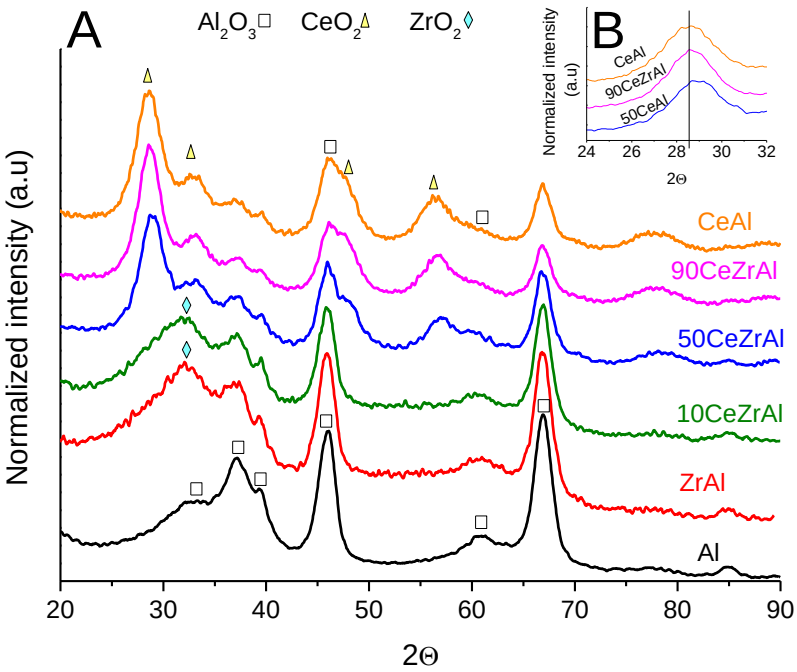

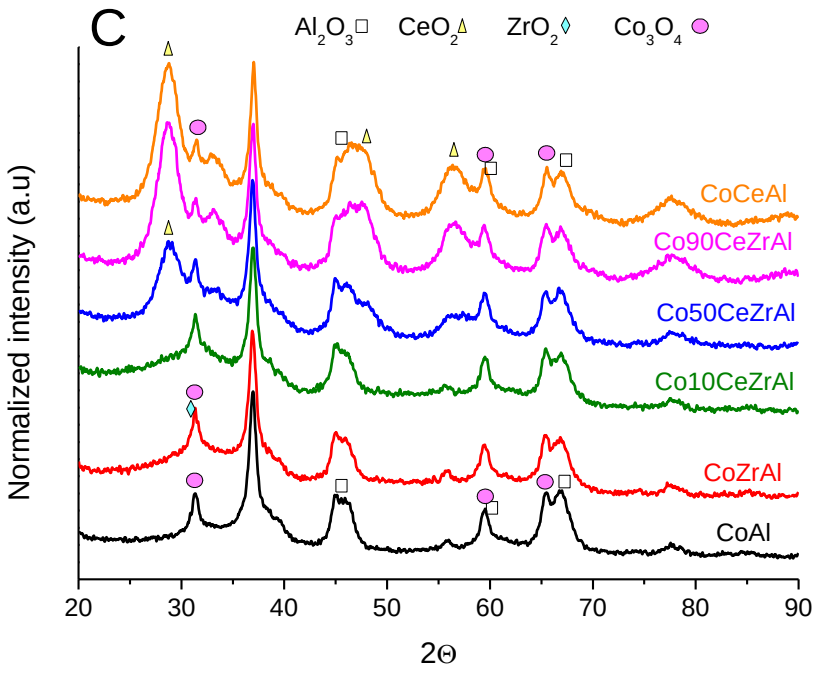

Figure 2. XPS spectra of the Al(2p) and Co(2p) core-levels of the CoAl and CoZrAl catalysts

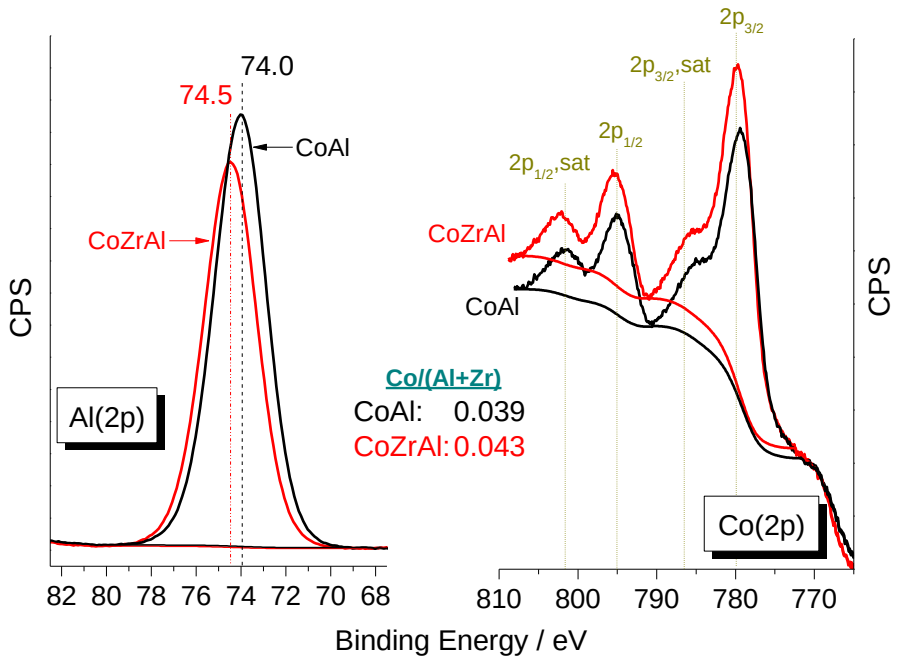

Figure 3. TPR profiles of the calcined catalysts: A) general TPR profiles; B) Extended view of the TPR profiles Zone I

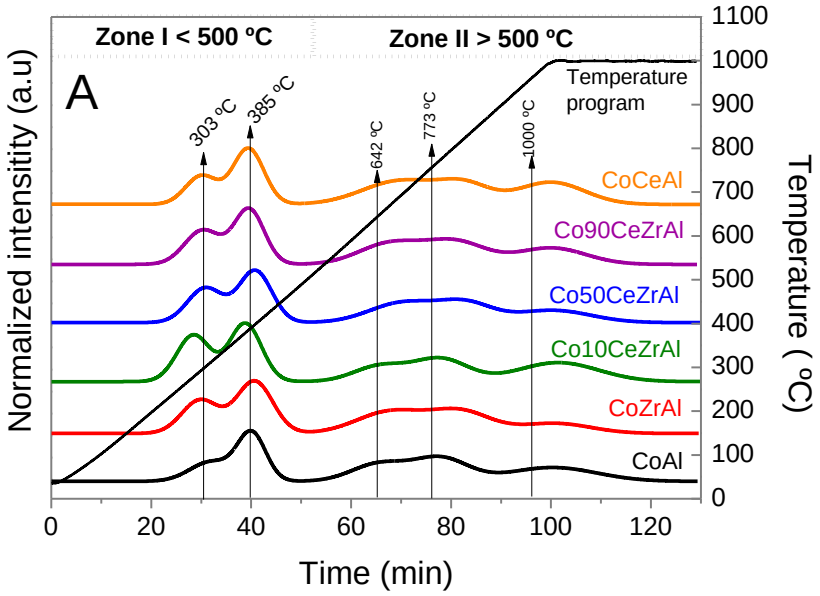

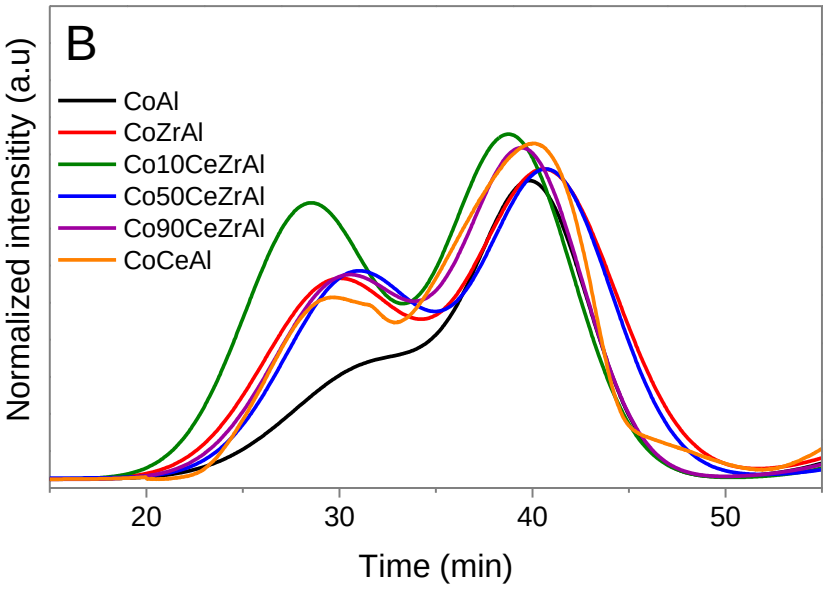

Figure 4. Catalytic activity during the Stage 1 (Comparison of the catalysts under the same space velocity)

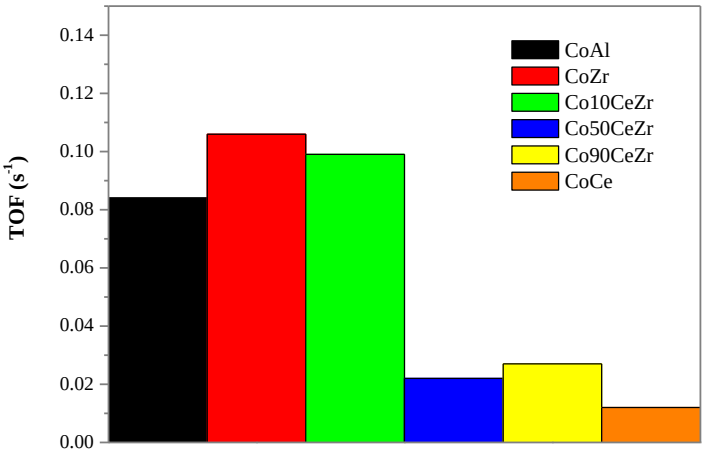

Figure 5. FTIR difference spectra of ZrAl support after the adsorption of small doses of CO in the v(OH) region (A) and the v(CO) region

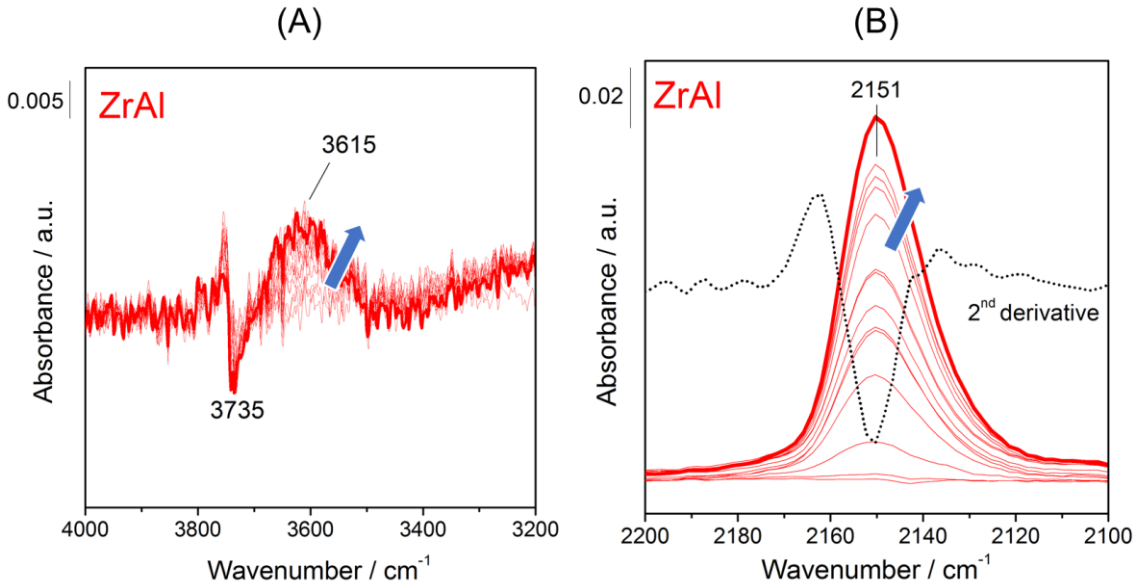

Figure 6. FTIR difference spectra of CeAl support after the adsorption of small doses of CO (OH) region (A) and the v(CO) regions. The inset shows the heat adsorption estimated for the adsorption of CO on the different Lewis acid sites

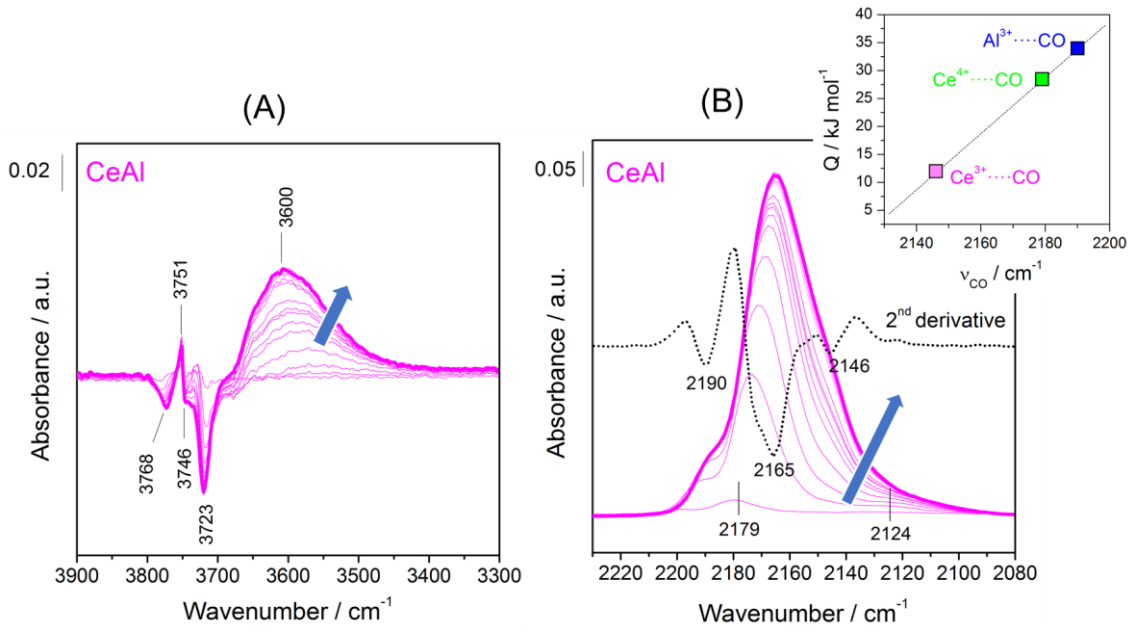

Figure 7. Effect of the inclusion of water within the feed-stream during the FTS. A) CO consumption rate; B) Selectivity to CH_4; C) Selectivity to C5+; D) Selectivity to CO_2; E) o/p ratio in C2; F) o/p ratio in C3; G) o/p ratio in C4

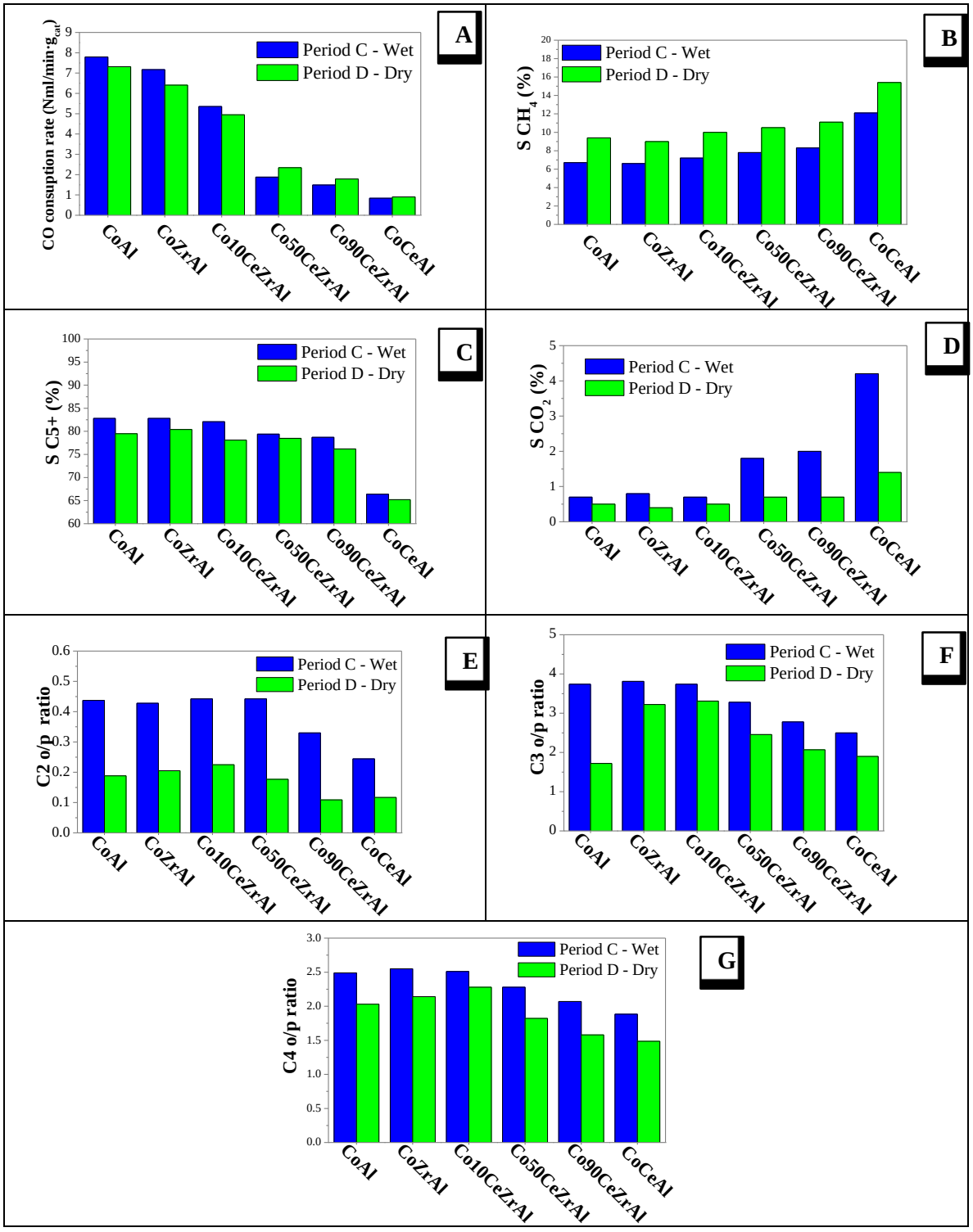
A
CO consuption rate (Nml/min·g$_{cat}$)
Period C - Wet
Period D - Dry
CoAl
CoZrAl
Co10CeZrAl
Co50CeZrAl
Co90CeZrAl
CoCeAl
B
S CH$_4$ (%)
C
S C5+ (%)
D
S CO$_2$ (%)
E
C2 o/p ratio
F
C3 o/p ratio
G
C4 o/p ratio